Unsteady aerodynamic modeling methodology based on dynamic mode interpolation for transonic flutter calculations

H. Güner[a,*], D. Thomas[a], G. Dimitriadis[a], V.E. Terrapon[a]

[a] *Aerospace and Mechanical Engineering Department, University of Liège, Quartier Polytech 1, Allée de la Découverte 9, 4000 Liège, Belgium*

Abstract

A new unsteady aerodynamic modeling methodology for calculating transonic flutter characteristics is presented. The main idea of the methodology is to obtain the unsteady flow response to small amplitude periodic deformations of a structure over a large range of oscillation frequencies through the interpolation of the most dominant fluid dynamic modes obtained from Dynamic Mode Decomposition (DMD) of a few reference unsteady simulations at different oscillation frequencies. These simulations can be carried out by solving the Euler or RANS equations. The methodology can then be used to obtain a frequency-domain generalized aerodynamic force matrix, and stability analysis can be performed using standard flutter analysis methods such as the p-k method. The proposed methodology provides a very good estimate of the flutter boundary for the 2D Isogai airfoil and 3D AGARD 445.6 wing models, but at a lower computational cost than the traditional higher-fidelity Fluid-Structure Interaction (FSI) simulations.

Keywords: unsteady aerodynamics, computational fluid dynamics, dynamic mode decomposition, transonic, flutter, aeroelasticity

*Corresponding author
Email address: hguner@uliege.be (H. Güner)

1. Introduction

The prediction of transonic flutter is of great importance to aircraft design as modern aircraft commonly fly at transonic conditions. However, the computation of the aeroelastic response of aircraft wings or control surfaces is challenging in this regime because transonic flows are characterized by aerodynamic nonlinearities such as moving shock waves. These nonlinear phenomena can result in unwanted aeroelastic effects and limit the performance of aircraft [1, 2].

The aerospace industry usually relies on unsteady panel methods based on the linearized potential equation, such as the Doublet-Lattice Method (DLM) [3], for routine aeroelastic analyses in preliminary design. Although these linear codes provide rapid and accurate predictions of the aerodynamic forces for purely subsonic or supersonic flows, they cannot capture the critical unsteady phenomena present in transonic flows (e.g., shock oscillations). This type of flow being inherently nonlinear, the full potential equation cannot be linearized even for small perturbations, and the aeroelastic calculations require higher-fidelity approaches.

Driven by the advance in computing power, different approaches have been proposed based on the Transonic Small Disturbance (TSD) equation, the full potential equation, the inviscid Euler equations, or the Reynolds-Averaged Navier-Stokes (RANS) equations [1, 4, 5, 6]. At the present time, the best option to accurately account for unsteady nonlinear aerodynamic phenomena is to directly solve the Euler or RANS equations. However, the use of Euler or RANS codes in industrial aeroelastic applications is limited due to the high computational cost required for repeated unsteady simulations

Several Reduced-Order Models (ROMs) of unsteady aerodynamic flows have been proposed (e.g., [7, 8, 9, 10, 11]). The main idea is to compute the eigenvalues and eigenmodes of a time or frequency-domain CFD model of unsteady flow. These eigenmodes are then used as basis vectors to construct a ROM with significantly fewer degrees of freedom than the original system, greatly decreasing the computational cost. The details of the formulation vary depending

on the level of fidelity of the fluid model, the technique used to determine the eigenvalues and eigenmodes, and the construction of the ROM. Among these variants, the popular ROMs using basis vectors determined from Proper Orthogonal Decomposition (POD) of unsteady flow solutions for prescribed wing motion at different frequencies can accurately compute the unsteady flow over a range of frequencies. These ROMs can predict the aeroelastic behavior of transonic airfoils [12], wings [13, 14, 15], and aircraft models [10, 16, 17] with decent accuracy.

This paper presents a conceptually novel unsteady aerodynamic modeling methodology, which is based on the interpolation of few dynamic modes obtained at only two different frequencies. The methodology can accurately predict the flutter characteristics of airfoils or wings in the transonic flow regime, and its computational cost is low enough to be applied to aeroelastic tailoring problems [18]. The proposed methodology has useful advantages over existing ROMs. In contrast to the above-mentioned ROMs, the methodology does not require the construction of a reduced-order approximation of the discretized governing equations. The interpolation of a few reference dynamic modes provides directly the generalized aerodynamic force matrix for a frequency range. Additionally, the methodology does not assume anything about the origin of the input flow data, so that it can be used with any fluid model and any existing CFD code or even with experimental measurements. Furthermore, the methodology can be used directly with standard flutter analysis techniques such as the widely used p-k method [19] to find the flutter characteristics of a system and also to describe its subcritical behavior.

The manuscript is organized as follows. Section 2 describes the proposed methodology. After a discussion of the main theoretical aspects in Section 2.1, each step of the methodology is illustrated in the case of a pitching airfoil in the transonic flow regime in Section 2.2. The proposed approach is then used in Section 3 to calculate the transonic flutter characteristics for two validation cases: the 2D Isogai airfoil and the 3D AGARD 445.6 wing. Finally, the main results are summarized and discussed in Section 4.

2. Methodology

The goal of the methodology is to provide the flow response to small amplitude periodic deformations of a structure as a function of the oscillation frequency for given flow conditions (Reynolds number Re and Mach number M). The main idea is to first perform a few high-fidelity unsteady CFD simulations, such as Euler or RANS simulations, with an imposed deformation at selected frequencies so as to capture the main nonlinear dynamic modes of the flow response. The second step then consists in interpolating these dynamic modes for any other frequency. The methodology is first described in more detail, and then illustrated for the case of a simple 2D airfoil.

2.1. Theoretical description

The first step of the methodology is to obtain the most relevant dynamic modes of the flow response to an imposed small-amplitude periodic structural deformation at a given frequency and for given flow conditions. One approach is to perform a high-fidelity simulation (Euler or RANS) of the flow around the oscillating structure and then post-process the results through Dynamic Mode Decomposition (DMD) [20, 21].

High-fidelity flow simulations provide the entire flow field around the oscillating structure as a function of time. After the initial transient phase, the unsteady flow fields can be processed using DMD in order to extract information about the flow response dynamics. DMD is applied to a time sequence of N flow fields represented by a matrix $\mathbf{V}$,

$$\mathbf{V} = \{\mathbf{v}_0, \mathbf{v}_1, \mathbf{v}_2, \ldots, \mathbf{v}_{N-1}\}, \tag{1}$$

where $\mathbf{v}_n$ denotes a vector representing the nth flow field. Two consecutive snapshots $\mathbf{v}_n$ and $\mathbf{v}_{n+1}$ are assumed to be separated by a constant time step Δt that must be small enough so that the relevant dynamic processes present in the flow response can be extracted from the input data sequence.

The application of the DMD procedure results in r modes, each mode consisting of an amplitude α_i, a spatial mode shape $\boldsymbol{\phi}_i(x, y, z)$, and a time behavior

given by the eigenvalue λ_i such that the flow field at a time instance n can be expressed as

$$\mathbf{v}_n = \sum_{i=0}^{r-1} \alpha_i \boldsymbol{\phi}_i \mathrm{e}^{\lambda_i n \Delta t}. \tag{2}$$

The real and imaginary parts of the mode eigenvalue λ_i represent respectively the rate of decay and frequency associated with this dynamic mode. If the unsteady flow has reached a fully established periodic state, then the real part of λ_i (decay) is zero. The modes that contribute most to the dynamics then need to be identified among all r modes. This is discussed in more detail in Section 2.2. In addition, assuming that the flow response to the periodic structural deformation is also periodic, the Harmonic Balance (HB) method [22, 8, 23] can be used to provide directly the fully-established periodic dynamics, which can reduce the computational cost. In this particular case, the time behavior of any conservation variable can be expressed as a sum of Fourier modes, which are comparable to the dynamic modes extracted from DMD of unsteady simulations.

The proposed methodology aims to obtain the flow response to an imposed periodic deformation of the structure at any oscillation frequency by interpolating the most dominant fluid dynamic modes obtained from a few high-fidelity reference simulations at different frequencies. The question is then to determine how many dynamic modes are required to capture the flow dynamics with sufficient accuracy, and what frequency should be imposed for the reference simulations. The objective of the following section is to analyze these two aspects and to illustrate each step of the methodology for a simple 2D NACA airfoil.

2.2. Transonic inviscid flow around a pitching NACA 64A010

All steps of the methodology are illustrated and two key aspects are analyzed: the relative contibution of the modes at a fixed forcing frequency and the influence of this forcing frequency on the fluid mode shapes.

The 2D transonic flow over a NACA 64A010 airfoil pitching around its quarter-chord point is used as a test case, based on the experiment by Davis [24].

This configuration has been chosen as it also enables the study of shocks that move due to structural oscillations. The free-stream Mach number M is 0.796 and the Reynolds number Re based on the chord c is 12.56×10^6. The pitching motion is specified as

$$\alpha(\tau) = \bar{\alpha} + \hat{\alpha} \sin(k\tau), \tag{3}$$

where $\alpha(\tau)$ is the variation of the angle of attack with non-dimensional time $\tau = tU_\infty/b$, U_∞ is the free-stream velocity, $b = c/2$, $\bar{\alpha}$ is the mean angle of attack, $\hat{\alpha}$ is the pitching amplitude, and the forcing reduced frequency is defined as $k = \omega b/U_\infty$ with ω the angular frequency. Unless otherwise specifically mentioned, all following results are obtained for $\bar{\alpha} = 0°$, $\hat{\alpha} = 1.01°$ and $k = 0.202$. As the mean angle of attack and pitching amplitude are small, the flow remains attached.

Only Euler simulations are considered in this work. They are carried out using the open-source CFD code SU2 [25, 26, 27]. The time-accurate simulation uses 25 time steps per period of oscillation to capture the relevant time scales, and the calculation is run until a periodic state has been reached to eliminate transient effects.

The boundaries of the computational domain are located about $50c$ away from the airfoil in order to minimize their impact on the solution in the region of interest. The computational grid corresponds to a C-type structured mesh with 200 points non-uniformly distributed around the airfoil and 54 points that are stretched in the normal direction. A grid convergence study has confirmed that this resolution is sufficient to provide accurate results, as illustrated by Figure 1. A similar resolution is used for the other Euler simulations presented in this article.

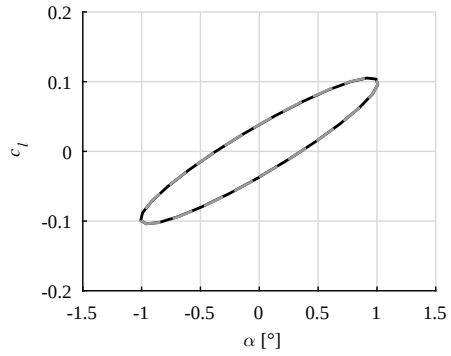

Figure 1: Lift coefficient c_l as a function of the angle of attack α obtained by unsteady Euler simulations for two levels of grid refinement: 200×54 (continuous gray line) and 400×108 (dashed black line).

Figure 2 shows three snapshots of the Mach field $M(x, y, \tau)$ at three instantaneous phase angles computed by an unsteady Euler simulation of the reference case, for $k = 0.202$. The shocks lie at the edge of the supersonic regions and their position clearly varies over time.

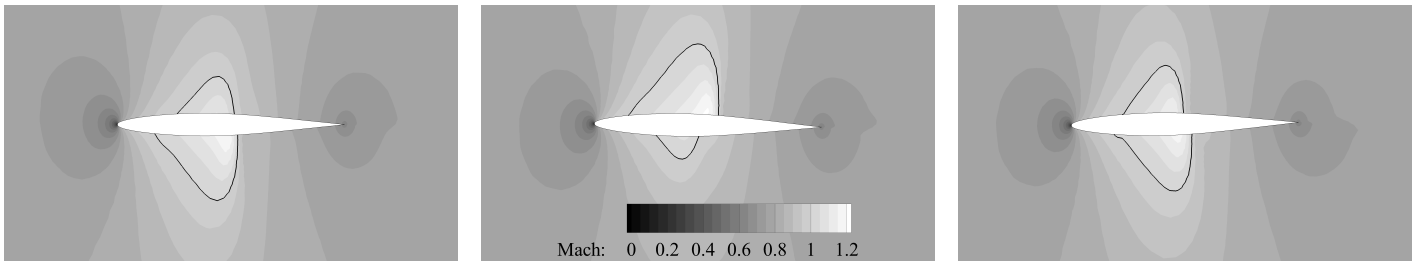

(a) $k\tau = 0°$ (b) $k\tau = 120°$ (c) $k\tau = 240°$

Figure 2: Contour of the Mach number at different phases of the forced oscillation cycle obtained by an unsteady Euler simulation. The black line represents $M = 1$.

Figure 3 shows that the variation of the lift coefficient c_l computed from the pressure fields and the chordwise position of the shock on the upper surface x_s extracted from the Mach fields obtained by the unsteady Euler simulation are in agreement with the experimental measurements for the reference conditions.

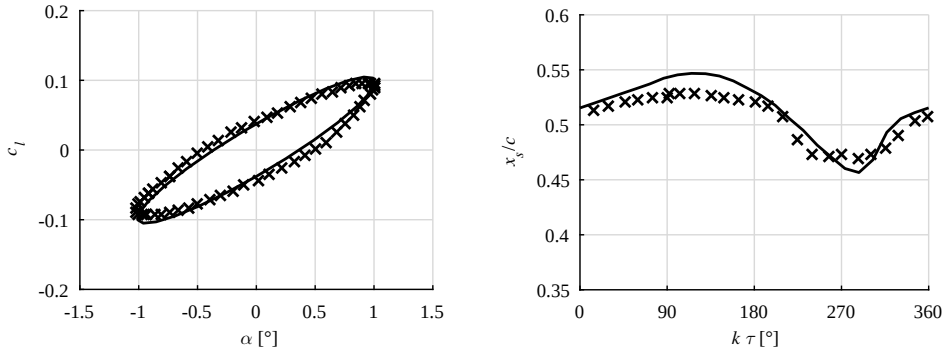

(a) Lift coefficient c_l

(b) Position of the shock on the upper surface x_s

Figure 3: Comparison of the unsteady Euler solution (continuous line) with the experimental data of Davis [24] (symbols) for the reference NACA 64A010 case pitching at reduced frequency $k = 0.202$.

As a first step, the dependence of the flow dynamics on the pitching frequency is assessed by comparing the results for several reduced frequencies k at the same nominal flow conditions. The pressure field is analyzed first as it is directly related to the aerodynamic forces, but the methodology could be applied to any other quantity. More specifically, DMD is applied to pressure coefficient fields generated by unsteady Euler simulations for three reduced frequencies $k = 0.1$, 0.202, and 0.3. The spatial size of the fields around the airfoil is chosen large enough to include the supersonic regions. The flow region used for DMD analysis is a rectangle of width $2c$ and height c centered on the airfoil. Only one period of oscillation is considered, i.e., the transient phase is discarded and 25 snapshots are used.

Figure 4 shows the resulting modal amplitude α_i against the corresponding modal frequency $\Im(\lambda_i)b/U_\infty$ of each DMD mode for the simulations carried out at the three values of k. Each modal amplitude distribution is discrete and symmetrical with respect to $\Im(\lambda_i) = 0$ because the input data is real [20]. Moreover, the eigenvalues are purely imaginary, i.e., there is no damping of the modes as the dynamics is fully periodic after the transient phase.

The highest peak represents the contribution of the mean flow, which is constant over time. The modal reduced frequency $\Im(\lambda_0)b/U_\infty$ associated with this mode is correspondingly zero. The second peak corresponds to the fundamental frequency, i.e., the frequency at which the pitching motion is forced, such that $\Im(\lambda_1)b/U_\infty = k$. The higher harmonics (i.e., integer multiples of the fundamental frequency) are well distinguishable, even at high k, but their amplitude decreases rapidly when the respective frequency $\Im(\lambda_i)b/U_\infty$ increases. Therefore, the modes at high $\Im(\lambda_i)b/U_\infty$ make a relatively small contribution to the flow dynamics. Note that the imposed pitching motion has here a small amplitude; cases with flow separation would not necessarily lead to the same result.

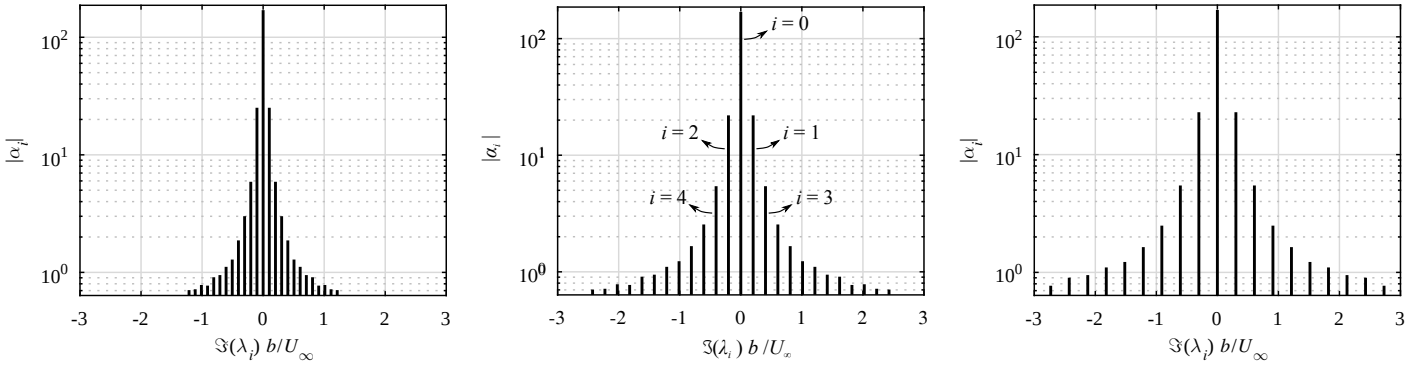

(a) $k = 0.1$ (b) $k = 0.202$ (c) $k = 0.3$

Figure 4: Absolute value of the modal amplitude α_i as a function of the corresponding modal reduced frequency $\Im(\lambda_i)b/U_\infty$ of the modes obtained from DMD of unsteady Euler pressure coefficient fields for the pitching NACA 64A010 case at three values of the reduced frequency k.

The time evolution of a flow field can be reconstructed from these DMD modes using Equation (2). On the other hand, a good approximation of the flow dynamics can be obtained by using only the most relevant DMD modes in the reconstruction. Figure 5 shows the variation of the aerodynamic lift and moment coefficients, c_l and c_m, computed from the reconstructed pressure field and the chordwise position of the shock x_s obtained from the reconstructed

Mach field using one and two modes, i.e., $r = 3$ and $r = 5$ in Equation (2) as each dynamic mode appears in pairs. In other words, the flow dynamics is reconstructed using the mean field and mode 1 corresponding to the pitching frequency (one-mode reconstruction) or, additionally, the first higher harmonic (two-mode reconstruction). The objective here is to analyze the accuracy of the solution with respect to the number of modes included in the reconstruction.

The lift and moment coefficients calculated using a single mode are already in very good agreement with the time-accurate unsteady solutions even at forcing frequencies that can be considered high in the context of flutter problems. Including the second mode does not really improve the results for the lift and moment coefficients. On the other hand, although a single mode provides already a relatively good prediction of the shock motion, including the second mode visibly improves the results.

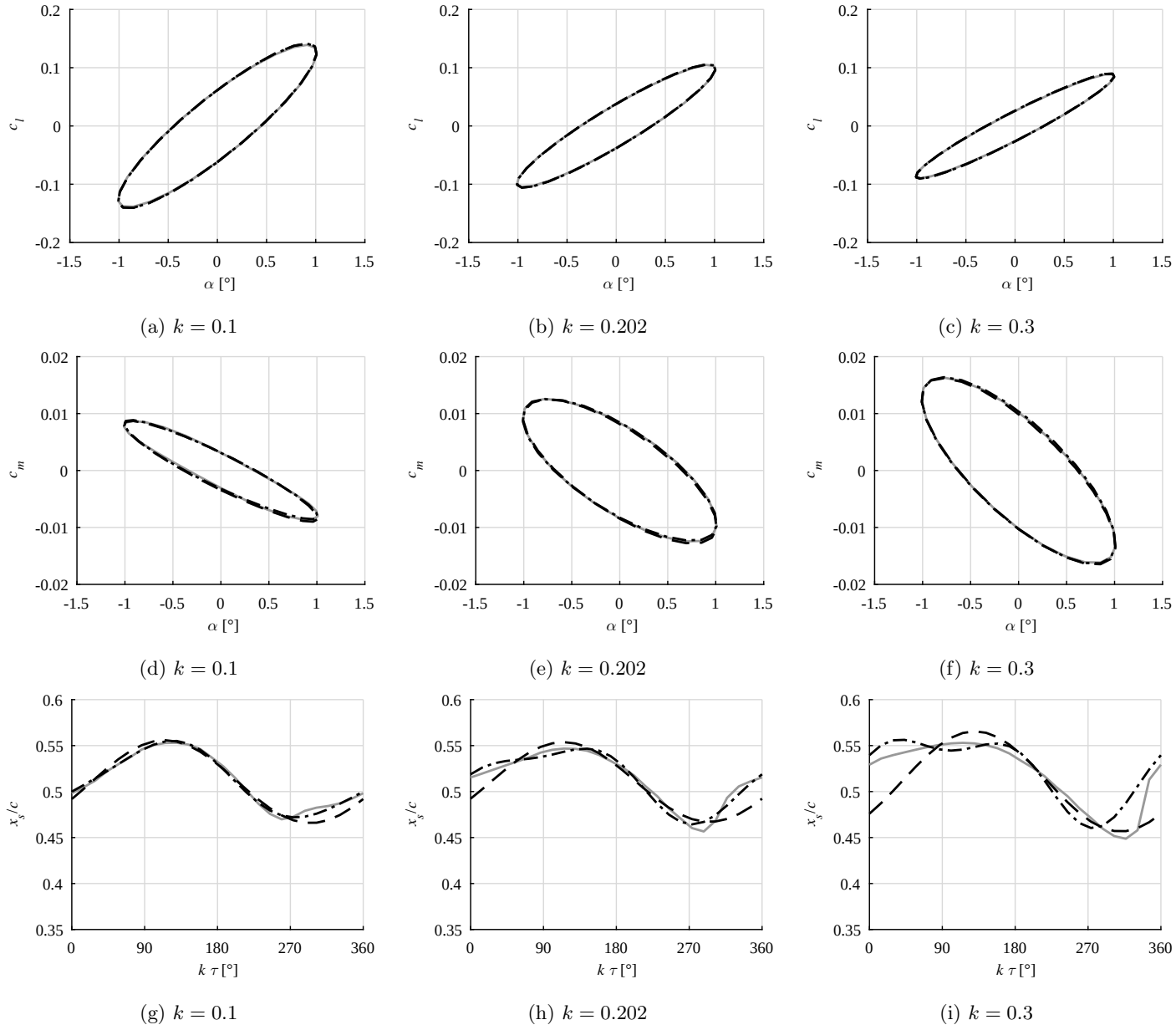

(a) $k = 0.1$ (b) $k = 0.202$ (c) $k = 0.3$

(d) $k = 0.1$ (e) $k = 0.202$ (f) $k = 0.3$

(g) $k = 0.1$ (h) $k = 0.202$ (i) $k = 0.3$

Figure 5: Comparison of lift coefficient c_l, moment coefficient c_m, and position of the shock on the upper surface x_s between the unsteady Euler solution (continuous gray line), the one-mode (dashed black line) and two-mode (dash-dotted black line) DMD representations for the pitching NACA 64A010 case at three values of the reduced frequency k.

Figure 6 illustrates the shape $\alpha_0\boldsymbol{\phi}_0$ of mode 0, i.e., the mean flow, as calculated from the three unsteady simulations at $k = 0.1$, 0.202, and 0.3. It shows that the DMD representation of the mean flow remains essentially independent of the pitching frequency k for such small-amplitude oscillations.

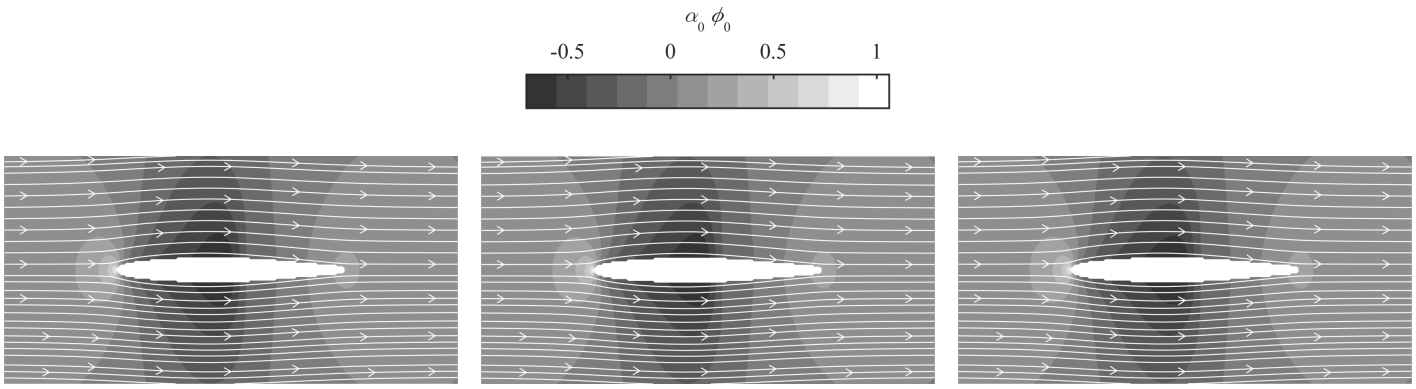

(a) $k = 0.1$ (b) $k = 0.202$ (c) $k = 0.3$

Figure 6: Influence of the reduced frequency k on the mean mode $\alpha_0\boldsymbol{\phi}_0$ extracted from unsteady Euler flow fields for the pitching NACA 64A010 case. The filled contour plots represent the mean pressure mode, and the streamlines represent the mean velocity mode.

Each dynamic mode is characterized by a spatial structure oscillating at a single frequency $\Im(\lambda_i)$. The first dynamic mode shown in Figure 7 oscillates at the fundamental frequency. Streamlines have been added to better visualize the mode shape, but one should keep in mind that these streamlines are not physical as the mean flow is not considered. It can be seen that the first dynamic mode changes progressively as k increases. The Modal Assurance Criterion (MAC) is used in order to demonstrate quantitatively this observation. The MAC is a technique used to compare mode shapes [28]. Considering two different spatial modes ϕ_A and ϕ_B, the MAC between these modes is calculated from

$$\mathrm{MAC}\left(\phi_A, \phi_B\right) = \left(\frac{\phi_A^T \phi_B}{\|\phi_A\| \, \|\phi_B\|}\right)^2. \tag{4}$$

By definition, the MAC is bounded between 0 and 1. If MAC is equal to 1, then the correlation is perfect; if MAC = 0, then the two modes are fully uncorrelated.

The MAC matrices shown in Figure 7 demonstrate that the correlation becomes weaker as the reduced frequencies are further apart. As a result, the dynamics of the flow in time, and hence the evolution of the shock waves that can profoundly affect the aeroelastic stability, will also change with k. It is thus important to account for these nonlinear effects.

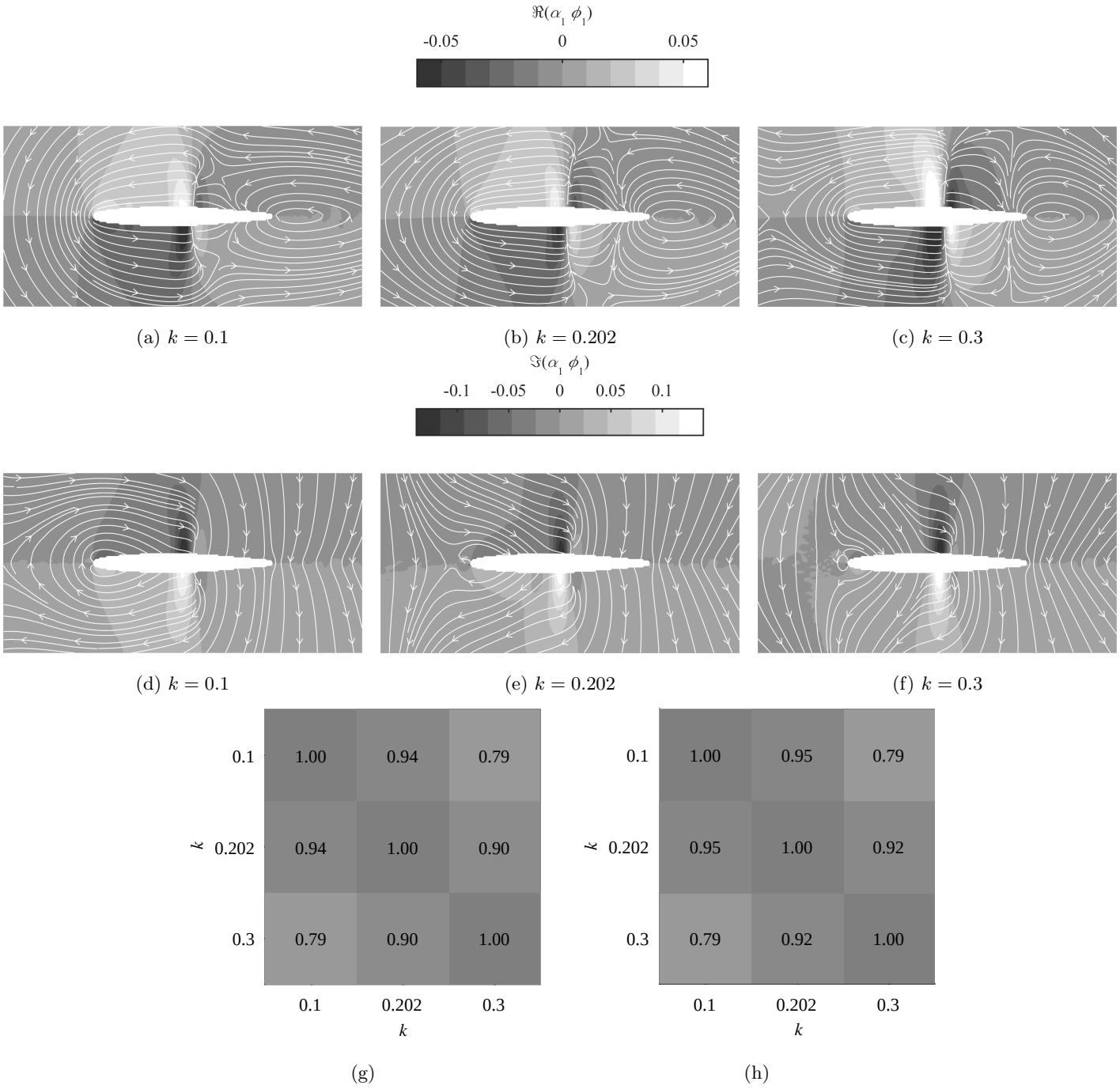

Figure 7: Influence of the reduced frequency k on (a–c) the real part and (d–f) the imaginary part of the first dynamic mode $\alpha_1 \boldsymbol{\phi}_1$ extracted from unsteady Euler flow fields for the pitching NACA 64A010 case. The filled contour plots represent the first pressure mode, and the streamlines represent the first velocity mode. MAC matrices comparing (g) the real part and (h) the imaginary part of the first dynamic velocity modes at three values of k.

DMD of unsteady Euler simulations has shown that only a few modes are important to capture the dynamical behavior of the inviscid transonic flow. The first dynamic mode, i.e., that corresponding to the frequency of the imposed motion, is sufficient to accurately estimate the lift and moment coefficients. Furthermore, the mode shapes change with the forcing frequency. It is thus important to capture this dependence on k for accurate flutter predictions.

DMD of an unsteady high-fidelity simulation provides the relevant modes for a given frequency of oscillation. If a different value of k is required, then another corresponding Euler (or RANS) simulation must be carried out. As a flutter analysis involves a large number of frequencies, this approach becomes computationally very expensive.

The idea of the proposed methodology is thus to compute the most dominant modes at two nearby reduced frequencies, and then estimate the dynamic modes corresponding to other frequencies through linear interpolation. This allows to account for the progressive changes in the mode shape with k at a limited cost. A linear relationship is used in this work, and it will be shown that this assumption gives satisfactory results for the present test cases and considered frequency ranges. Higher-order interpolations requiring more reference simulations could also be used to achieve higher accuracy at the expense of the computational cost.

As an example, the first dynamic modes of the pressure and velocity fields at $k = 0.202$ are obtained through interpolation between the corresponding modes at $k = 0.1$ and 0.3. Figure 8 compares the real and imaginary parts of this mode estimated by interpolation to the corresponding exact mode for both the pressure coefficient (contour) and the velocity field (streamlines). Good agreement can be observed. This is quantitatively confirmed by the corresponding MAC values which are very close to 1: MAC = 0.97 for the real parts and MAC = 0.99 for the imaginary parts.

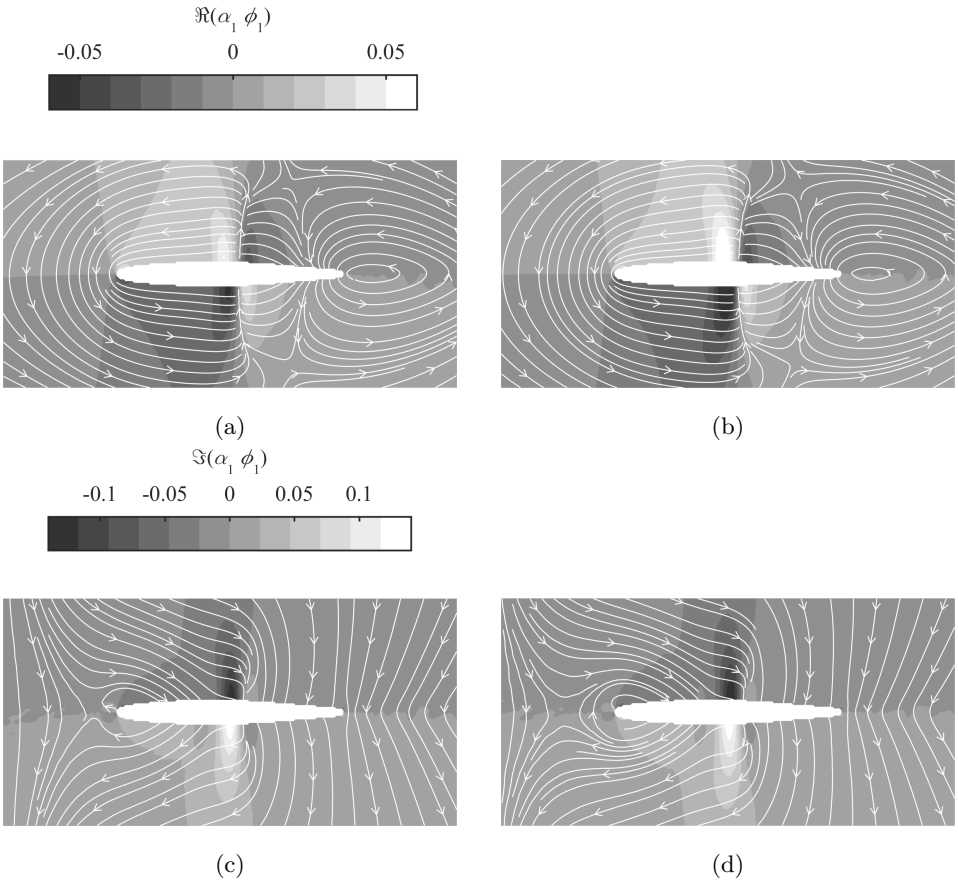

Figure 8: (a) Real part and (c) imaginary part of the first dynamic mode $\alpha_1\boldsymbol{\phi}_1$ at $k = 0.202$ extracted from unsteady Euler flow fields for the pitching NACA 64A010 case. (b) Real part and (d) imaginary part of the first dynamic mode at $k = 0.202$ interpolate from the first dynamic modes at $k = 0.1$ and 0.3. The filled contour plots represent the first pressure mode, and the streamlines represent the first velocity mode.

In Figure 9, the resulting lift and moment coefficients and the shock location from mode interpolation are compared to the corresponding results using the exact modes at $k = 0.202$ and the unsteady Euler solution. Again, the dynamic mode interpolation approach provides good results, even with a single mode.

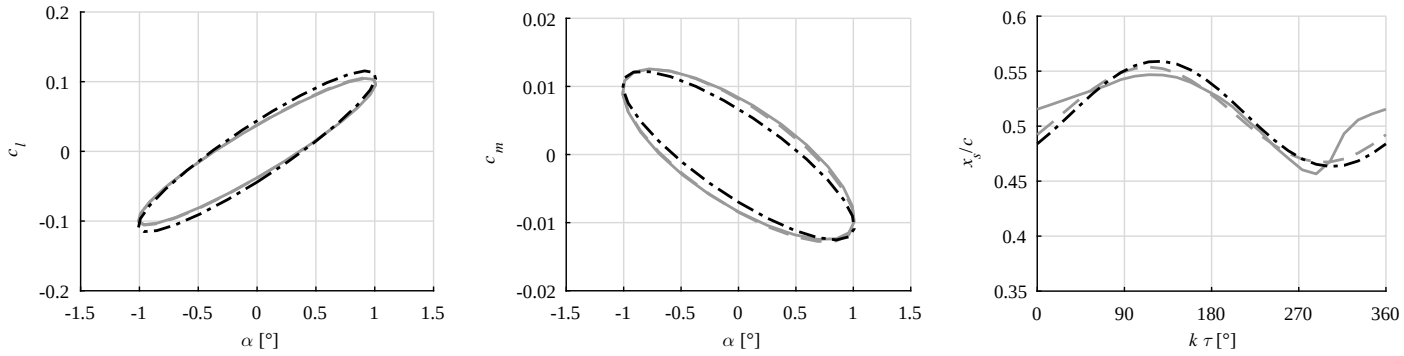

(a) Lift coefficient c_l (b) Moment coefficient c_m (c) Position of the shock on the upper surface x_s

Figure 9: Comparison of the unsteady Euler solution (continuous gray line), the one-mode DMD representation (dashed gray line), and the present dynamic mode interpolation approach (dash-dotted black line) based on the first dynamic modes at $k = 0.1$ and 0.3 for the reference pitching NACA 64A010 case at reduced frequency $k = 0.202$.

More generally, for small amplitude simple harmonic motions, interpolating from the solutions at $k = 0.1$ and 0.3 provides good estimations of the most dominant modes, and hence of the complete flow dynamics, over a frequency range, provided that the frequency is not much larger than the higher reference forcing frequency. From a computational point of view, only two unsteady simulations are sufficient here.

3. Applications to transonic flutter calculations

In this section, the methodology is applied to the stability analysis of a 2D airfoil model and a 3D wing model in order to test its performance for predicting the onset of transonic flutter.

3.1. Isogai wing section

As illustrated in Figure 10, the Isogai wing section model [29] consists in a 2D airfoil with two degrees of freedom; it can undergo a combination of pitching (α) and plunging (h) motion. The aeroelatic equation for the system is given

by

$$\mathbf{M}\begin{pmatrix}\ddot{h}(t)\\ \ddot{\alpha}(t)\end{pmatrix}+\mathbf{K}\begin{pmatrix}h(t)\\ \alpha(t)\end{pmatrix}=\begin{pmatrix}-l(t)\\ m(t)\end{pmatrix}, \tag{5}$$

where $\mathbf{M}$ and $\mathbf{K}$ are the mass and stiffness matrices of the structure, respectively, l is the aerodynamic lift, and m is the aerodynamic moment about the elastic axis. The geometry is a NACA 64A010 airfoil, which is the same as for the pitching airfoil test case studied in Section 2.2. All the structural parameters shown in Figure 10, on which the mass and stiffness matrices directly depend, are known from Isogai [29]. On the other hand, the aerodynamic forces depend on the dynamics of the airfoil and are not explicitly known because of the nonlinearity of the problem.

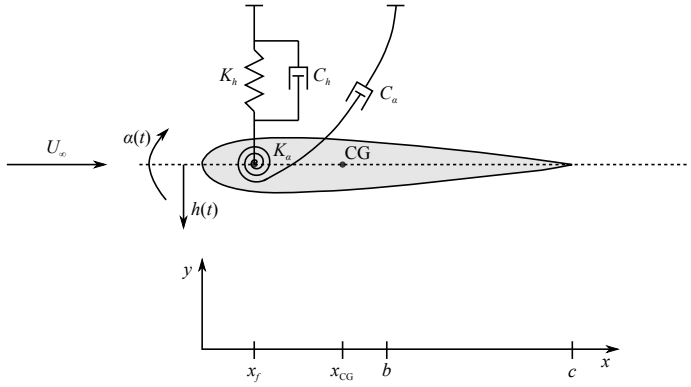

Figure 10: Typical two-degree-of-freedom wing section aeroelastic model. (Adapted from Reference [30].)

The dynamic mode interpolation approach is thus used to model the fluid flow, and more specifically the aerodynamic forces. Assuming a sinusoidal motion of the airfoil and a resulting oscillating lift and moment, and separating the contribution of the plunging and pitching motion for small amplitudes, the aeroelastic equation becomes

$$\left(-\left(\frac{kU_\infty}{b}\right)^2\mathbf{M}+\mathbf{K}\right)\begin{pmatrix}\hat{h}\\ \hat{\alpha}\end{pmatrix}\mathrm{e}^{ik\tau}=\begin{pmatrix}\frac{-\hat{l}_{\mathrm{plunge}}(k)}{\hat{h}} & \frac{-\hat{l}_{\mathrm{pitch}}(k)}{\hat{\alpha}}\\ \frac{\hat{m}_{\mathrm{plunge}}(k)}{\hat{h}} & \frac{\hat{m}_{\mathrm{pitch}}(k)}{\hat{\alpha}}\end{pmatrix}\begin{pmatrix}\hat{h}\\ \hat{\alpha}\end{pmatrix}\mathrm{e}^{ik\tau}, \tag{6}$$

where $\hat{l}_{\text{plunge}}$ and $\hat{m}_{\text{plunge}}$ denote the lift and moment amplitudes due to a plunging motion of amplitude $\hat{h}$, and $\hat{l}_{\text{pitch}}$ and $\hat{m}_{\text{pitch}}$ represent those due only to a pitching motion of amplitude $\hat{\alpha}$. In general, for a sinusoidal motion, the amplitude of the aerodynamic forces depends not only on the flow conditions and the reduced frequency k but also on the pitching and plunging amplitudes $\hat{\alpha}$ and $\hat{h}$. However, if small oscillations of the geometry are considered, the amplitude of the aerodynamic forces are linear in the amplitude of the airfoil motion, $\hat{\alpha}$ and $\hat{h}$, so that the aerodynamic forces only depend on the reduced frequency of oscillation and the flow conditions.

Equation (3.1) can also be expressed in terms of the aerodynamic coefficients c_l and c_m:

$$\left(-\left(\frac{kU_\infty}{b}\right)^2\mathbf{M}+\mathbf{K}\right)\begin{pmatrix}\hat{h}\\ \hat{\alpha}\end{pmatrix}\mathrm{e}^{ik\tau}=\frac{1}{2}\rho U_\infty^2\underbrace{\begin{pmatrix}\frac{-c\,\hat{c}_{l_{\text{plunge}}}(k)}{\hat{h}} & \frac{-c\,\hat{c}_{l_{\text{pitch}}}(k)}{\hat{\alpha}}\\ \frac{c^2\,\hat{c}_{m_{\text{plunge}}}(k)}{\hat{h}} & \frac{c^2\,\hat{c}_{m_{\text{pitch}}}(k)}{\hat{\alpha}}\end{pmatrix}}_{\mathbf{Q}_1(k)}\underbrace{\begin{pmatrix}\hat{h}\\ \hat{\alpha}\end{pmatrix}\mathrm{e}^{ik\tau}}_{\mathbf{q}(k)}, \tag{7}$$

where ρ is the air density, U_∞ is the free-stream velocity, and c is the airfoil chord. This expression can be written in a more general form by introducing the vector of degrees of freedom in the frequency domain $\mathbf{q}(k)$ and the aerodynamic force matrix $\mathbf{Q}(k)=1/2\rho U_\infty^2\mathbf{Q}_1(k)\mathbf{q}(k)$:

$$\left(-\left(\frac{kU_\infty}{b}\right)^2\mathbf{M}+\mathbf{K}-\frac{1}{2}\rho U_\infty^2\mathbf{Q}_1(k)\right)\mathbf{q}(k)=\mathbf{0}. \tag{8}$$

The aerodynamic parameters $\hat{c}_{l_{\text{pitch}}}$ and $\hat{c}_{m_{\text{pitch}}}$ are calculated using the following steps:

- First, a given free-stream Mach number M and two reference pitching frequencies are chosen. The present calculation uses $k=0.1$ and 0.3 because flutter typically occurs at reduced frequencies of the order of 0.1 in most transonic flutter problems encountered in aircraft wings or control surfaces [1]. Additionally, the methodology has to accurately capture the unsteady nonlinear aerodynamic effects over a certain range of k.

- The next step consists in obtaining the first dynamic mode of the pressure field for a forced pitching motion through DMD of unsteady Euler simulations at the two frequencies chosen above and small pitching amplitude $\hat{\alpha}$. A small amplitude is sufficient for flutter analysis. The present calculation uses $\hat{\alpha} = 1°$.

- The first dynamic pressure mode is then obtained at any other frequency through interpolation between the two reference frequencies.

- From the interpolated dynamic pressure mode, the lift and moment coefficients are calculated at any frequency and normalized by the amplitude $\hat{\alpha}$ of the imposed pitching motion.

The entire procedure can be repeated for the plunging motion. The plunging amplitude $\hat{h}$ is set to $0.1c$ here. Finally, matrix $\mathbf{Q}$ can thus be computed for a given Mach number using only four unsteady Euler simulations.

Because of its dependence on the frequency, Equation (8) corresponds to a nonlinear eigenvalue problem. The flutter condition can be determined directly through the p-k method [31]. This flutter prediction algorithm gives the variations of the natural reduced frequencies k_i and damping ratios ζ_i of the system as a function of the speed index $V_\infty = U_\infty/(b\omega_\alpha\sqrt{\mu})$, where U_∞ is the free-stream speed, b the airfoil semi-chord, ω_α the natural frequency of the section in pitch, and $\mu = m/(\pi\rho b^2)$ the airfoil mass ratio. Flutter occurs when at least one of the system damping ratios is equal to zero. The speed index at which this occurs is the flutter speed index V_f.

Although the Isogai aeroelastic problem is two-dimensional, computing its flutter boundary is challenging. This is due to the nonlinearity inherent to the transonic flow regime. In particular, the flutter speed is lower in the transonic regime compared to the subsonic and supersonic regimes. This transonic dip illustrated in Figure 11 is caused by moving shock waves [1]. This phenomenon can only be modeled by taking into account the flow nonlinearities. For instance, linear codes, such as those using the doublet lattice method, highly overpredict the flutter speed in the transonic regime, which can lead to an inappropriate

and unsafe design. Note that the thickness distribution of the airfoil has also an important impact on the unsteady aerodynamic forces, and must be taken into account. Furthermore, the Isogai aeroelastic problem presents multiple bifurcations.

The flutter boundary obtained by applying the p-k method in conjunction with the proposed dynamic mode interpolation methodology is represented by the filled circles in Figure 11. Comparison with reference results from the literature [32, 33, 12, 30] based on unsteady Euler simulations of the full Fluid-Structure Interaction (FSI) problem demonstrates that the present methodology provides a very good estimate of the flutter boundary. The transonic dip is accurately predicted, and the multiple flutter points in the range $0.85 < M < 0.9$ (approximately) are well captured.

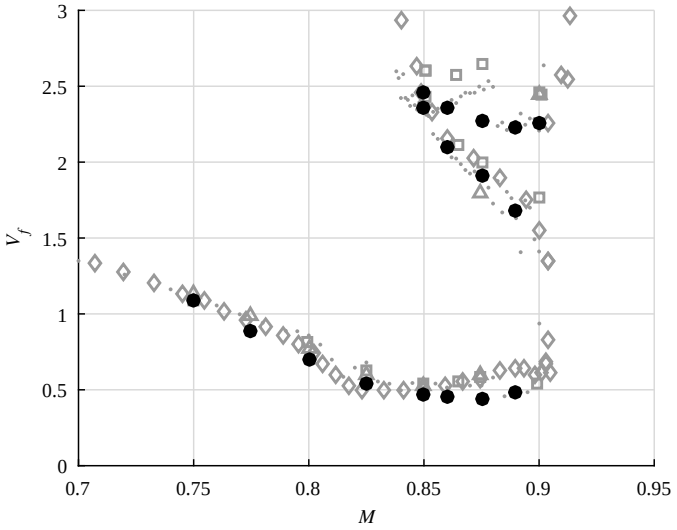

Figure 11: Flutter boundary (flutter speed index V_f as a function of the Mach number M) for the Isogai wing section obtained with the present methodology (filled circles) and compared to time-accurate aeroelastic simulations using the Euler equations: Timme and Badcock [32] (dots), Yang *et al.* [33] (squares), Hall *et al.* [12] (diamonds), Alonso *et al.* [30] (triangles).

Figure 12 illustrates three characteristic flutter behaviors:

- For $M = 0.75$, the system is stable (both damping ratios are positive) until

the speed index reaches the flutter speed index $V_f = 1.09$. The single flutter mode is the plunging mode, and the associated flutter reduced frequency $k_{f1} = 0.14$.

- For $M = 0.875$, the aeroelastic problem presents several flutter points. The first one is triggered by the plunging mode at $V_f = 0.44$ and $k_{f1} = 0.23$. Time-accurate aeroelastic solutions also reveal that the flutter mode at the bottom of the transonic dip is the plunging mode [30]. The system is unstable from $V_\infty = 0.44$ to 1.91. The system becomes stable again between $V_\infty = 1.91$ and 2.25 as both damping ratios are positive. Then, the damping ratio of the pitching mode vanishes at $V_f = 2.25$, and the associated reduced frequency $k_{f2} = 0.27$ is higher than the previous flutter point. The system is unstable beyond this flutter speed index. The flutter mode is the pitching mode for this upper unstable branch of the flutter boundary, which is consistent with the reference results.

- For $M = 0.9$, the pitching mode is the only flutter mode. It appears at high frequency ($k_{f2} = 0.28$).

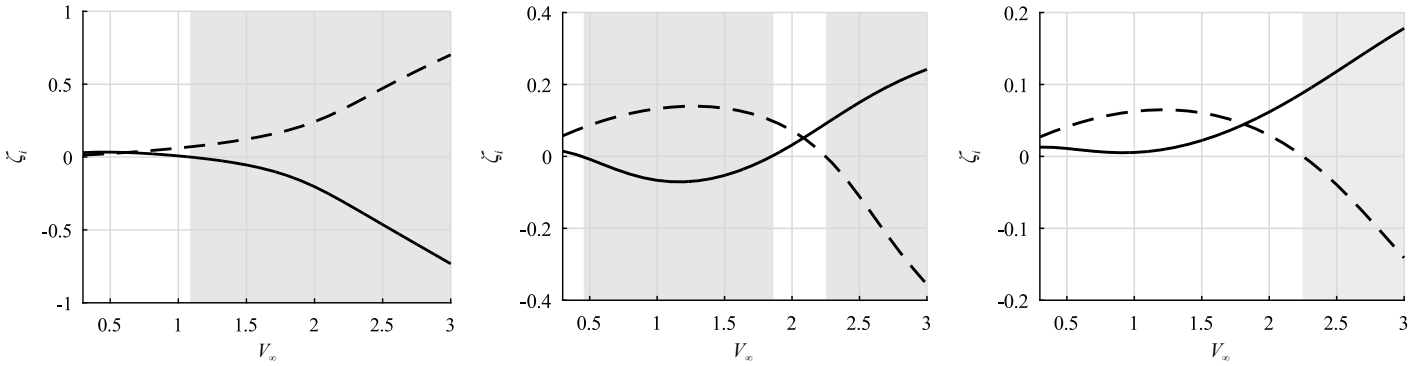

(a) $M = 0.75$ (b) $M = 0.875$ (c) $M = 0.9$

Figure 12: Damping ratios ζ_i associated with the plunge (continuous line) and pitch (dashed line) degrees of freedom obtained by the *p-k* method in conjunction with the present methodology based on the interpolation of dynamic modes for three different Mach numbers showing three different characteristic flutter behaviors.

These results are in agreement with the time-accurate aeroelastic reference solutions. However, some discrepancies are observed for the upper unstable branch of the flutter boundary between the present results and the reference data from the literature, but also among these reference results (see Figure 11). These differences may have different origins. First, the computational meshes might differ, introducing numerical errors. Note that in the present case, a careful mesh-refinement analysis has been performed for the high-fidelity simulations used as basis for the interpolation. The CFD mesh used in this section has 21760 quadrilaterals. The boundaries of the computational domain are far from the region of interest in order to minimize their impact on the solution, and the mesh is finer near the airfoil. Second, the interpolation operation used in the present methodology to obtain matrix $\mathbf{Q}$ can introduce an error. The choice of the reference frequencies can be verified a posteriori based on the analysis results. In this case, our choice ($k = 0.1$ and 0.3) includes all k of interest, since flutter occurs at reduced frequencies between 0.14 and 0.28. Finally, the time step used in the unsteady Euler simulations from the literature might be

too large, introducing numerical errors. The main reason is that most of these works have based their time step on a low reduced frequency. The simulations of the pitching mode flutter on the upper unstable branch, for which the reduced frequency is much higher, are thus most likely under-resolved in time [30]. In the present case, 25 snapshots are taken per period, even for the simulations at $k = 0.3$, so that the dominant modes are every time adequately resolved. Nonetheless, these discrepancies at high reduced frequency are not excessively critical since the first flutter point appearing at lower speed index is usually the one constraining the design and is accurately estimated. The proposed method provides good results at lower cost.

3.2. AGARD 445.6 wing

The generalization of the methodology to a 3D case is quite straightforward. Figure 13 gives an overview of the main practical steps of the methodology. This section illustrates each step for the case of the 3D AGARD 445.6 wing [34].

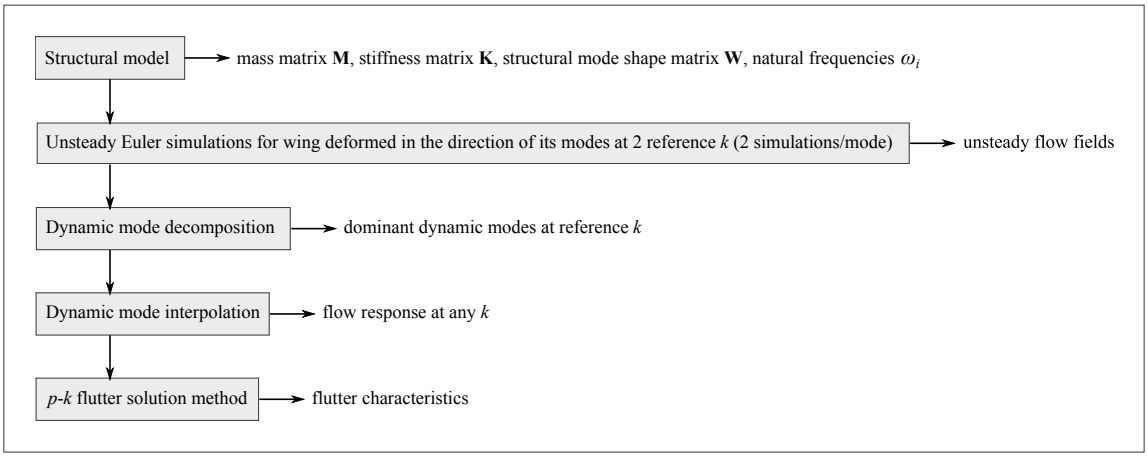

Figure 13: Main practical steps of the methodology.

The model considered here corresponds to the weakened wall-mounted semi-span model 3 of Yates *et al.* [34]. The aspect ratio of the wing is 1.6525, its taper ratio is 0.6576, its quarter-chord sweepback is 45°, and the section is a

NACA 65A004 airfoil. A finite element model constucted using the finite element package Metafor [35] is used to obtain the mass matrix $\mathbf{M}$, the stiffness matrix $\mathbf{K}$, the mode shape matrix $\mathbf{W} = \{\mathbf{w}_1, \mathbf{w}_2, \ldots, \mathbf{w}_{n_d}\}$ that contains the mode shapes $\mathbf{w}_i$, and the natural frequencies. Matrices $\mathbf{M}$, $\mathbf{K}$, and $\mathbf{W}$ are all square matrices of size $n_d \times n_d$ with n_d the total number of degrees of freedom contained in the finite element model.

The first four modes of vibration of the structure extracted from the finite element model and the associated natural frequencies are shown in Figure 14. Mode 1 is the first bending mode, mode 2 is the first torsional mode, and modes 3 and 4 combine both bending and torsion.

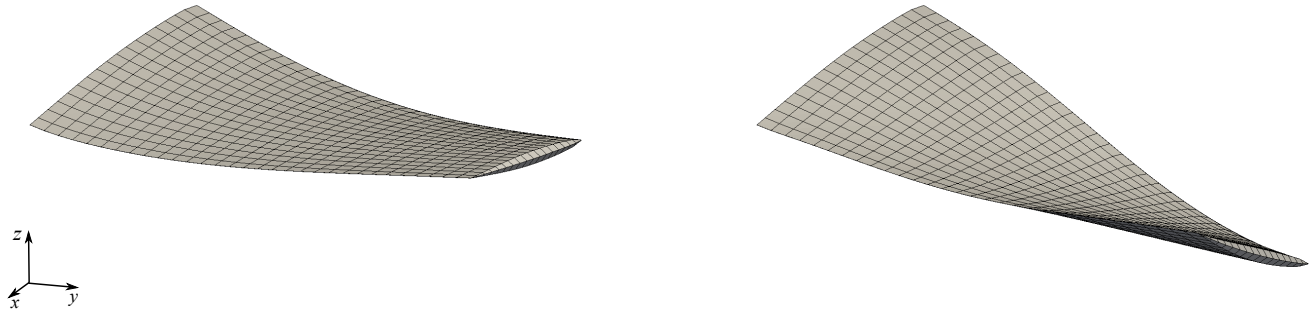

(a) Structural mode 1 (9.54 Hz)

(b) Structural mode 2 (40.35 Hz)

(c) Structural mode 3 (50.22 Hz)

(d) Structural mode 4 (97.67 Hz)

Figure 14: First four finite element modes of vibration and corresponding frequency on the structural grid for the AGARD 445.6 wing model.

Using a modal model for the structure and considering only a few vibration mode shapes, the modal aeroelastic equations can be expressed as

$$\left(-\left(\frac{kU_\infty}{b}\right)^2 \mathbf{A} + \mathbf{E} - \frac{1}{2}\rho U_\infty^2 \mathbf{Q}_{r1}(k)\right)\mathbf{r}(k) = \frac{1}{2}\rho U_\infty^2 \mathbf{Q}_{r0}, \tag{9}$$

where b is half the mean aerodynamic chord $\bar{c}$, $\mathbf{A} = \mathbf{W}_r^T \mathbf{M} \mathbf{W}_r$ is the $n_r \times n_r$ reduced modal mass matrix with $\mathbf{W}_r$ the $n_d \times n_r$ truncated structural mode shape matrix that retains only the first n_r modes, $\mathbf{E} = \mathbf{W}_r^T \mathbf{K} \mathbf{W}_r$ is the $n_r \times n_r$ reduced modal stiffness matrix, and $\mathbf{r}(k)$ is the $n_r \times 1$ reduced generalized coordinates vector in the frequency domain. The reduced modal frequency-domain

generalized aerodynamic force matrix $\mathbf{Q}_r(k)$ can be computed as explained in Dimitriadis [36, 37]:

$$\mathbf{Q}_r(k) = \frac{1}{2}\rho U_\infty^2 \left(\mathbf{Q}_{r0} + \mathbf{Q}_{r1}(k)\mathbf{r}(k)\right), \tag{10}$$

where

$$\mathbf{Q}_{r1}(k) = \left(\mathbf{N}(k)^T \mathbf{W}_r\right)^T, \tag{11}$$

$\mathbf{N}(k)$ is a $n_d \times n_r$ matrix that contains the aerodynamic normal forces acting on the structural grid points of the wing due to imposed modal deformation specified by $\mathbf{W}_r$ (e.g., the first column of $\mathbf{N}(k)$ corresponds to the contribution due to the first bending mode). The free-stream velocity being along the x axis, the normal forces are applied to the z degree of freedom of each node of the structural grid.

The present aerodynamic modeling methodology based on dynamic mode interpolation is used to calculate the aerodynamic loads. Each chosen mode of vibration is interpolated linearly from the structural grid (1230 nodes on the wing surface) to the CFD mesh (6280 nodes on the wing surface). The numerical tool CUPyDO [38] is used to transfer the structural mode shape to the CFD code SU2. For each chosen mode, two unsteady Euler simulations are carried out for the wing oscillating parallel to the selected mode at two different forcing frequencies, $k = 0.05$ and $k = 0.2$. Similarly to the 2D case discussed in Section 3.1, a small-amplitude sinusoidal motion is assumed in each chosen mode. The maximum wing deflection is set to $0.08\,\bar{c}$ here.

The reference unsteady Euler simulations generate the unsteady flow fields that can be processed using DMD in order to obtain the reference dynamic modes. Following the guidelines of Section 2.2, only the first dynamic modes are considered in the dynamic mode interpolation procedure to estimate the flow response at any k. This assumption is verified in Figure 15 where the variation of the lift coefficient of the AGARD 445.6 wing due to forced modal deformations at $k = 0.1$ is estimated from interpolation of the reference first dynamic pressure modes for $k = 0.05$ and 0.2. It can be seen that the solutions based on one interpolated DMD mode are in good agreement with the exact

unsteady Euler solutions at $k = 0.1$ for both bending and torsion modes of the wing.

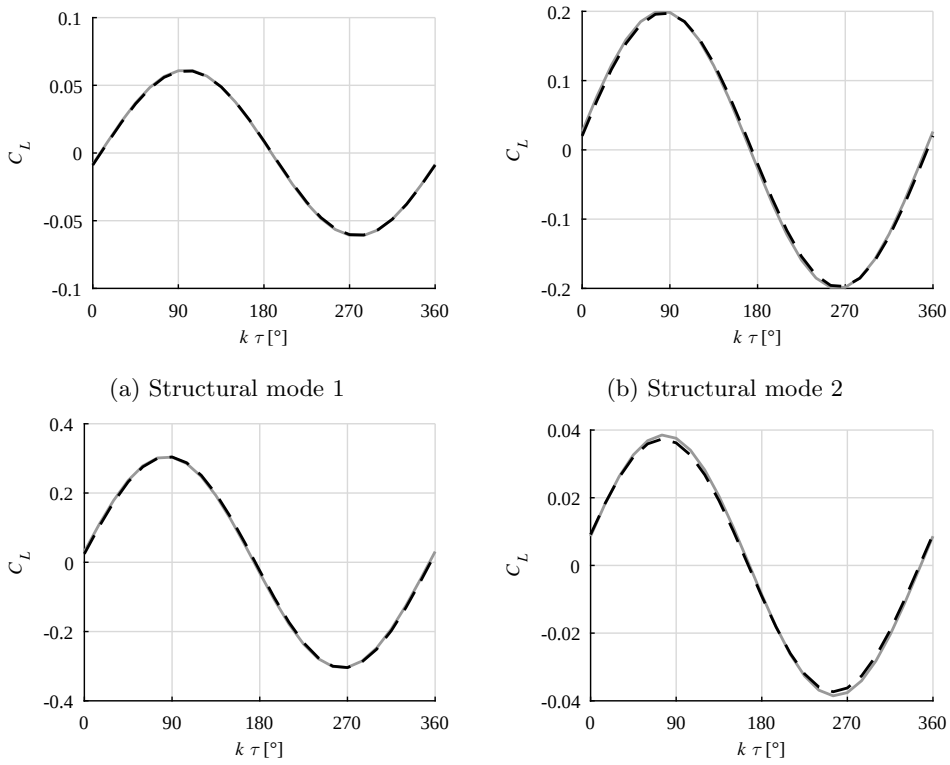

(a) Structural mode 1

(b) Structural mode 2

(c) Structural mode 3

(d) Structural mode 4

Figure 15: Comparison of the unsteady Euler solutions (continuous gray line) with the present dynamic mode interpolation approach (dashed black line) using the first dynamic pressure modes at two reference reduced frequencies $k = 0.05$ and 0.2 to predict the lift coefficient C_L of the AGARD 445.6 wing oscillating in the direction of its modes of vibration at $k = 0.1$ and a free-stream Mach number $M = 0.9$. The first four modes of vibration are considered. The maximum deflection is $0.08\,\bar{c}$ for each mode.

In order to obtain matrix $\mathbf{Q}(k)$, the resulting pressure field is interpolated from the CFD mesh to the structural grid. The aerodynamic normal force contribution of each structural grid element can then be calculated from the pressure field. In the present case, the wing camber, dihedral angle, and mean angle of attack being zero, $\mathbf{Q}_0 = 0$. Standard flutter analysis techniques such

as the p-k method can then be used to perform a stability analysis.

Figure 16 demonstrates that the transonic flutter boundary computed by the present methodology is in agreement with the numerical flutter data from the literature at the same Mach numbers and mass ratios. Moreover, considering only two structural modes of vibration (mode 1 and 2) is sufficient to predict the flutter onset accurately. The first bending mode, which has the lowest natural frequency, is the flutter mode for all considered Mach numbers. Since the method can only be as good as a CFD analysis, one can observe discrepancies with experimental results at high Mach numbers similar to other numerical studies.

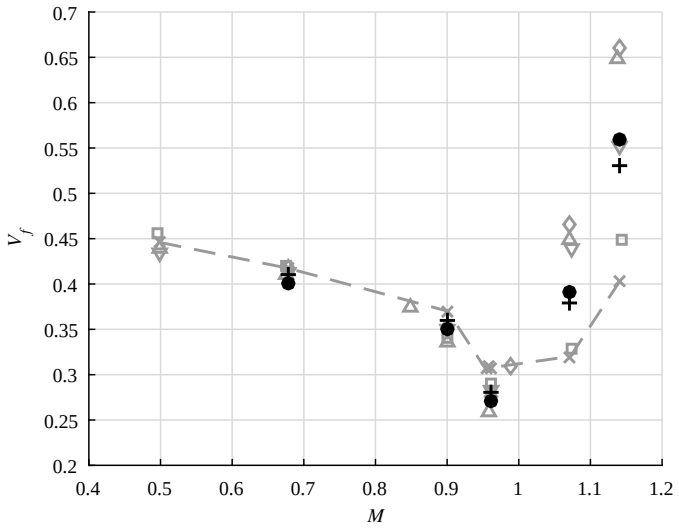

Figure 16: Flutter boundary (flutter speed index V_f as a function of the Mach number M) for the AGARD 445.6 wing obtained with the present methodology using 4 (filled circles) or 2 (plus signs) structural mode shapes, and compared to experimental flutter data [34] (dashed line with crosses) and time-accurate aeroelastic simulations using the Euler equations: Chen *et al.* [39] (squares), Lee and Batina [40] (diamonds), Liu *et al.* [41] (upward-pointing triangles), Thomas *et al.* [38] (downward-pointing triangles).

The computational time to simulate 4 periods of oscillation is about 3.2 hours on 16 cores (Intel E5-2650 processors at 2.0 GHz) using a CFD mesh with 248000 hexahedra. For example, if two modes of vibration are considered,

the methodology requires 4 unsteady Euler simulations per Mach number to estimate the flutter speed. The procedure to obtain the modal frequency-domain generalized force matrix and the application of the p-k flutter solution algorithm only take a few minutes. The present methodology is thus computationally much more efficient than the traditional approach based on higher-fidelity FSI simulations, while providing a similar level of accuracy.

4. Conclusions

The relevant dynamics of the flow around a structure undergoing small-amplitude periodic forced motion can be estimated over an entire range of oscillation frequencies by interpolating the most dominant fluid dynamic modes from reference solutions computed at two nearby frequencies. It has been shown that the first mode, whose frequency corresponds to the oscillation frequency, is sufficient for the test cases considered here. This approach can significantly decrease the computational cost compared to repeated time-accurate simulations while still accounting for the relevant dynamics, such as the motion of shocks, even at relatively high frequency. It should also be noted that the most relevant dynamic modes can also be directly obtained from harmonic balance simulations, instead of applying DMD to unsteady Euler simulations, which could in many cases further reduce the computational cost.

The p-k method combined with this dynamic mode interpolation approach is able to accurately predict the transonic dip due to moving shocks and multiple flutter points in the case of a two-dimensional aeroelastic pitch-plunge configuration, but at a lower computational cost than the traditional higher-fidelity Fluid-Structure Interaction (FSI) simulations. Moreover, the methodology has been extended to three-dimensional wings, for which the AGARD aeroelastic problem has been used as first validation case. In this context, the methodology also provides accurate flutter predictions, even with only a few vibration modes.

Overall, the proposed methodology represents a promising approach for accurate but still fast flutter calculations, even in the transonic flow regime. Al-

though the method has so far only relied on Euler simulations, thus excluding effects linked to the nonlinear interaction between the shock and the viscous boundary layer, the extension of the methodology to RANS simulations should be straightforward and will be the focus of future work.

5. Acknowledgements

The authors gratefully acknowledge the aerospace company Embraer S.A. for supporting this research. Computational resources have been provided by the Consortium des Équipements de Calcul Intensif (CÉCI), funded by the Fonds de la Recherche Scientifique de Belgique (F.R.S.-FNRS) under Grant No. 2.5020.11.

References

[1] O. O. Bendiksen, Review of unsteady transonic aerodynamics: theory and applications, Progress in Aerospace Sciences 47 (2) (2011) 135–167.

[2] G. A. Vio, G. Dimitriadis, J. E. Cooper, K. J. Badcock, M. A. Woodgate, A. M. Rampurawala, Aeroelastic system identification using transonic CFD data for a wing/store configuration, Aerospace Science and Technology 11 (2) (2007) 146–154.

[3] E. Albano, W. P. Rodden, A doublet-lattice method for calculating lift distributions on oscillating surfaces in subsonic flows., AIAA Journal 7 (2) (1969) 279–285.

[4] J. T. Batina, Efficient algorithm for solution of the unsteady transonic small-disturbance equation, Journal of Aircraft 25 (7) (1988) 598–605.

[5] T. L. Holst, Transonic flow computations using nonlinear potential methods, Progress in Aerospace Sciences 36 (1) (2000) 1–61.

[6] P. A. Durbin, B. P. Reif, Statistical theory and modeling for turbulent flows, 2nd Edition, John Wiley & Sons, 2011.

[7] E. H. Dowell, K. C. Hall, M. C. Romanowski, Eigenmode analysis in unsteady aerodynamics: Reduced order models, Applied Mechanics Reviews 50 (6) (1997) 371–386.

[8] D. J. Lucia, P. S. Beran, W. A. Silva, Reduced-order modeling: new approaches for computational physics, Progress in Aerospace Sciences 40 (1-2) (2004) 51–117.

[9] W. A. Silva, R. E. Bartels, Development of reduced-order models for aeroelastic analysis and flutter prediction using the CFL3Dv6.0 code, Journal of Fluids and Structures 19 (6) (2004) 729–745.

[10] T. Kim, M. Hong, K. G. Bhatia, G. SenGupta, Aeroelastic model reduction for affordable computational fluid dynamics-based flutter analysis, AIAA Journal 43 (12) (2005) 2487–2495.

[11] E. H. Dowell, H. C. Curtiss, R. H. Scanlan, F. Sisto, A modern course in aeroelasticity, 5th Edition, Springer, 2015.

[12] K. C. Hall, J. P. Thomas, E. H. Dowell, Proper orthogonal decomposition technique for transonic unsteady aerodynamic flows, AIAA Journal 38 (10) (2000) 1853–1862.

[13] J. P. Thomas, E. H. Dowell, K. C. Hall, Three-dimensional transonic aeroelasticity using proper orthogonal decomposition-based reduced-order models, Journal of Aircraft 40 (3) (2003) 544–551.

[14] T. Lieu, M. Lesoinne, Parameter adaptation of reduced order models for three-dimensional flutter analysis, in: 42nd AIAA Aerospace Sciences Meeting and Exhibit, 2004, p. 888.

[15] J. P. Thomas, E. H. Dowell, K. C. Hall, Static/dynamic correction approach for reduced-order modeling of unsteady aerodynamics, Journal of Aircraft 43 (4) (2006) 865–878.

[16] D. Amsallem, C. Farhat, Interpolation method for adapting reduced-order models and application to aeroelasticity, AIAA Journal 46 (7) (2008) 1803–1813.

[17] P. Hu, M. Bodson, M. Brenner, Towards real-time simulation of aeroservoelastic dynamics for a flight vehicle from subsonic to hypersonic regime, in: AIAA Atmospheric Flight Mechanics Conference and Exhibit, 2008, p. 6375.

[18] M. H. Shirk, T. J. Hertz, T. A. Weisshaar, Aeroelastic tailoring-theory, practice, and promise, Journal of Aircraft 23 (1) (1986) 6–18.

[19] H. J. Hassig, An approximate true damping solution of the flutter equation by determinant iteration., Journal of Aircraft 8 (11) (1971) 885–889.

[20] P. J. Schmid, Dynamic mode decomposition of numerical and experimental data, Journal of Fluid Mechanics 656 (2010) 5–28.

[21] M. R. Jovanović, P. J. Schmid, J. W. Nichols, Sparsity-promoting dynamic mode decomposition, Physics of Fluids 26 (2) (2014) 024103.

[22] K. C. Hall, J. P. Thomas, W. S. Clark, Computation of unsteady nonlinear flows in cascades using a harmonic balance technique, AIAA Journal 40 (5) (2002) 879–886.

[23] S. Nimmagadda, T. D. Economon, J. J. Alonso, C. R. Ilario da Silva, Robust uniform time sampling approach for the harmonic balance method, in: 46th AIAA Fluid Dynamics Conference, 2016-3966.

[24] S. S. Davis, NACA 64A010 (NASA Ames model) oscillatory pitching, AGARD Report 702 (1982).

[25] F. Palacios, M. R. Colonno, A. C. Aranake, A. Campos, S. R. Copeland, T. D. Economon, A. K. Lonkar, T. W. Lukaczyk, T. W. Taylor, J. J. Alonso, Stanford University Unstructured (SU2): An open-source integrated computational environment for multi-physics simulation and design, AIAA Paper 287 (2013).

[26] F. Palacios, T. D. Economon, A. C. Aranake, S. R. Copeland, A. K. Lonkar, T. W. Lukaczyk, D. E. Manosalvas, K. R. Naik, A. S. Padrón, B. Tracey, et al., Stanford University Unstructured (SU2): Open-source analysis and design technology for turbulent flows, AIAA Paper 243 (2014) 13–17.

[27] T. D. Economon, F. Palacios, S. R. Copeland, T. W. Lukaczyk, J. J. Alonso, Su2: An open-source suite for multiphysics simulation and design, AIAA Journal 54 (3) (2015) 828–846.

[28] R. Allemang, D. Brown, A correlation coefficient for modal vector analysis, in: Proceedings of the 1st International Modal Analysis Conference, 1982, pp. 110–116.

[29] K. Isogai, On the transonic-dip mechanism of flutter of a sweptback wing, AIAA Journal 17 (7) (1979) 793–795.

[30] J. Alonso, A. Jameson, Fully-implicit time-marching aeroelastic solutions, in: 32nd Aerospace Sciences Meeting and Exhibit, 1994, p. 56.

[31] W. P. Rodden, E. D. Bellinger, Aerodynamic lag functions, divergence, and the british flutter method, Journal of Aircraft 19 (7) (1982) 596–598.

[32] S. Timme, K. Badcock, Transonic aeroelastic instability searches using sampling and aerodynamic model hierarchy, AIAA Journal 49 (6) (2011) 1191–1201.

[33] S. Yang, Z. Zhang, F. Liu, S. Luo, H.-M. Tsai, D. Schuster, Time-domain aeroelastic simulation by a coupled euler and integral boundary-layer method, in: 22nd Applied Aerodynamics Conference and Exhibit, 2004, p. 5377.

[34] E. C. Yates, N. S. Land, J. T. Foughner, Measured and calculated subsonic and transonic flutter characteristics of a 45 sweptback wing planform in air and in Freon-12 in the Langley transonic dynamics tunnel, National Aeronautics and Space Administration, 1963.

[35] Metafor. A nonlinear finite element code, University of Liège. http://metafor.ltas.ulg.ac.be/, accessed May 16, 2018.

[36] G. Dimitriadis, Introduction to Nonlinear Aeroelasticity, 1st Edition, John Wiley & Sons, 2017.

[37] G. Dimitriadis, N. Giannelis, G. Vio, A modal frequency-domain generalised force matrix for the unsteady Vortex Lattice method, Journal of Fluids and Structures 76 (2018) 216–228.

[38] D. Thomas, M. L. Cerquaglia, R. Boman, T. Economon, J. Alonso, G. Dimitriadis, V. Terrapon, CUPyDO - An integrated Python environment for coupled fluid-structure simulations, Advances in Engineering Software (accepted).

[39] X. Chen, G.-C. Zha, M.-T. Yang, Numerical simulation of 3-D wing flutter with fully coupled fluid–structural interaction, Computers & Fluids 36 (5) (2007) 856–867.

[40] L. Elizabeth M, B. John T, Calculation of AGARD wing 445.6 flutter using Navier-Stokes aerodynamics, NASA Langley Technical Report Server (1993).

[41] F. Liu, J. Cai, Y. Zhu, H. Tsai, A. F. Wong, Calculation of wing flutter by a coupled fluid-structure method, Journal of Aircraft 38 (2) (2001) 334–342.